Cloud Vertical Structure and Its Variations from a 20-Yr Global Rawinsonde Dataset

JUNHONG WANG

*National Center for Atmospheric Research, Boulder, Colorado**

WILLIAM B. ROSSOW

NASA Goddard Institute for Space Studies, New York, New York

YUANCHONG ZHANG

Department of Applied Physics and Mathematics, Columbia University, New York, New York

(Manuscript received 8 February 1999, in final form 8 September 1999)

ABSTRACT

A global cloud vertical structure (CVS) climatic dataset is created by applying an analysis method to a 20-yr collection of twice-daily rawinsonde humidity profiles to estimate the height of cloud layers. The CVS dataset gives the vertical distribution of cloud layers for single and multilayered clouds, as well as the top and base heights and layer thicknesses of each layer, together with the original rawinsonde profiles of temperature, humidity, and winds. The average values are cloud-top height = 4.0 km above mean sea level (MSL), cloud-base height = 2.4 km MSL, cloud-layer thickness = 1.6 km, and separation distance between consecutive layers = 2.2 km. Multilayered clouds occur 42% of the time and are predominately two-layered. The lowest layer of multilayered cloud systems is usually located in the atmospheric boundary layer (below 2-km height MSL). Clouds over the ocean occur more frequently at lower levels and are more often formed in multiple layers than over land. Latitudinal variations of CVS also show maxima and minima that correspond to the locations of the intertropical convergence zone, the summer monsoons, the subtropical subsidence zones, and the midlatitude storm zones. Multilayered clouds exist most frequently in the Tropics and least frequently in the subtropics; there are more multilayered clouds in summer than in winter. Cloud layers are thicker in winter than in summer at mid- and high latitudes, but are thinner in winter in Southeast Asia.

1. Introduction

Clouds and the general circulation of earth's atmosphere are linked in an intimate feedback loop, where clouds result from the water vapor transports and cooling by atmospheric motions, but the forcing for the atmospheric circulation is significantly modified by vertical and horizontal gradients in radiative and latent heat fluxes induced by the clouds (e.g., Webster and Stephens 1984). To determine the importance of this feedback for climate change, we need quantitative measurements of the geographic distribution and variations of cloud vertical structure (CVS) to diagnose the processes involved. Despite a long record of surface cloud observations (Warren et al. 1986, 1988), globally complete measurements of clouds over the whole range of atmospheric motion scales from convective scale to planetary wave scale did not become available until the advent of weather satellites (see references in Hughes 1984; Rossow 1993). Both these observing systems provide information about the horizontal and vertical distribution of clouds (Hahn et al. 1982, 1984; Warren et al. 1985; Rossow and Schiffer 1991; Wylie and Wang 1997), but their vertical distribution statistics are sampling-limited by ''obscuration'' effects: the surface observer sees only the lowermost cloud layer in a column while the satellite sees only the uppermost cloud layer, requiring so-called overlap assumptions about layers not seen to estimate the complete CVS. Little direct information about CVS exists.

Changes of CVS (locations of cloud top and base, number and thickness of layers) affect the atmospheric circulations in atmospheric general circulation models (GCMs) by modifying the distribution of radiative and

* The National Center for Atmospheric Research is sponsored by the National Science Foundation.

Corresponding author address: Dr. Junhong Wang, NCAR/SSSF, P.O. Box 3000, Boulder, CO 80307-3000.
E-mail: junhong@ucar.edu

latent heating rates within the atmosphere (e.g., Slingo and Slingo 1988; Randall et al. 1989; Slingo and Slingo 1991; Wang and Rossow 1998). Wang and Rossow (1998) concluded that the three most important CVS parameters are the location of the top of the uppermost cloud layer, the presence or absence of multiple cloud layers, and the separation distance between two consecutive layers in multilayered cloud systems. They also found that vertical gradients in the cloud distribution were somewhat more important to the circulation strength in their model than horizontal gradients (cf. Rind and Rossow 1984). However, the nature of the cloud–circulation interactions in these GCM experiments needs to be verified by observations; in particular, to determine the model vertical resolution required to represent the distribution of cloud layer thicknesses, the effects of clear-air separations between cloud layers, and the importance of resolving the in-cloud radiative heating profile with net heating in the lower part and net cooling in upper part of the cloud layer (e.g., Stephens 1978; Wang and Rossow 1998).

Most available satellite measurements from nadir-pointing instruments are limited to retrieval of information about the uppermost cloud layer or column-integral properties, but some information about CVS may be obtained by multispectral approaches for particular situations (e.g., Baum et al. 1994; Jin and Rossow 1997; Sheu et al. 1997; Lin et al. 1998). A more promising approach uses active sensors, such as lidars (Sassen 1991; Platt et al. 1994) and cloud radars (Kropfli et al. 1995) or both (Uttal et al. 1995; Wang et al. 1999), to profile cloud layers from the surface; however, these approaches cannot provide complete global coverage and have not yet been employed on satellites.

Rawinsonde data have received increased attention in climate research because of its long record (the last four or five decades) and extensive coverage (best in the Northern Hemisphere). Rawinsonde measurements of the vertical profiles of temperature and humidity as they *penetrate* cloud layers can also provide information about the vertical distribution of clouds by identifying saturated levels in the atmosphere. Poore et al. (1995) combined 14 years (1975–88) of rawinsonde and surface observations from 63 sites in the Northern Hemisphere to create a climatic dataset of cloud layer thicknesses. Wang and Rossow (1995, hereinafter WR95) developed an improved analysis method that uses the rawinsonde observations (raobs) alone to determine CVS (section 2). This paper presents the first comprehensive description of the vertical distribution of cloud layers obtained from an analysis of a 20-yr (1976–95) collection of daily rawinsonde data from all available surface sites (section 3). Section 4 summarizes the near-global statistics of CVS, highlighting land–ocean contrasts and latitudinal and seasonal variations. Last, in section 5, the observed CVS variations are discussed in relation to the issues mentioned above.

2. Data and analysis method

a. Rawinsonde data

Available rawinsonde data provide twice-daily observations of upper-atmospheric conditions (temperature, humidity, winds, pressure) spanning a 20-yr period (1976–95): the first 15 years are obtained from the Geophysical Fluid Dynamics Laboratory of the National Oceanic and Atmospheric Administration (Peixoto and Oort 1996) and the last 5 years come from the rawinsonde archives at the National Center for Atmospheric Research. The dataset comes from about 1200 stations around the globe (Fig. 1) with most stations providing observations at 0000 and 1200 UTC and only about 100–200 stations also providing data at 0600 and 1800 UTC. The stations in South America lack observations at 0000 UTC; those in Australia lack observations at 1200 UTC (Fig. 1). The number of stations decreases to about 700 after excluding those on ships in the Atlantic and Pacific (Fig. 1). Sixty-eight percent out of a total of 1164 stations at 1200 UTC in January report at least 10 observations per month for more than 15 years (Fig. 1).

The analysis method described below is applied to the rawinsonde dataset to generate a ''global'' CVS dataset that also includes the original rawinsonde parameters. The CVS parameters consist of the number of cloud layers, base and top heights, and layer thickness for each layer, and the index of the levels where the cloud tops and bases are located to give the temperature and humidity at the cloud boundaries and within.

Raobs report temperature, humidity, wind speed, and wind direction as a function of height above MSL at mandatory, significant, generated, and some additional levels (such as the tropopause and maximum wind level) from surface to the maximum observation altitude. Humidity is variously reported as relative humidity (RH) with respect to liquid water, specific humidity, or dewpoint depression with respect to liquid water. We convert all humidity parameters to RH with respect to liquid water at temperatures $\geq 0°C$ and with respect to ice at temperatures $< 0°C$. The minimum observation pressure (maximum altitude) and the vertical resolution of raobs vary from sounding to sounding, even at the same site, and affect the quality of the CVS dataset (see details in section 3b); on average, the minimum pressure is 269 mb (a maximum altitude of about 11 km) and the vertical resolution is 53 mb.

b. Rawinsonde analysis to determine CVS

The analysis method to determine CVS is described in detail in WR95 and briefly outlined here. Cloudy layers are associated with RH values above 84% as the rawinsonde penetrates the layer, but the maximum RH within the cloud must be at least 87%. Cloud layer top and base locations are identified by RH jumps $>3\%$ (positive at the base and negative at the top, respec-

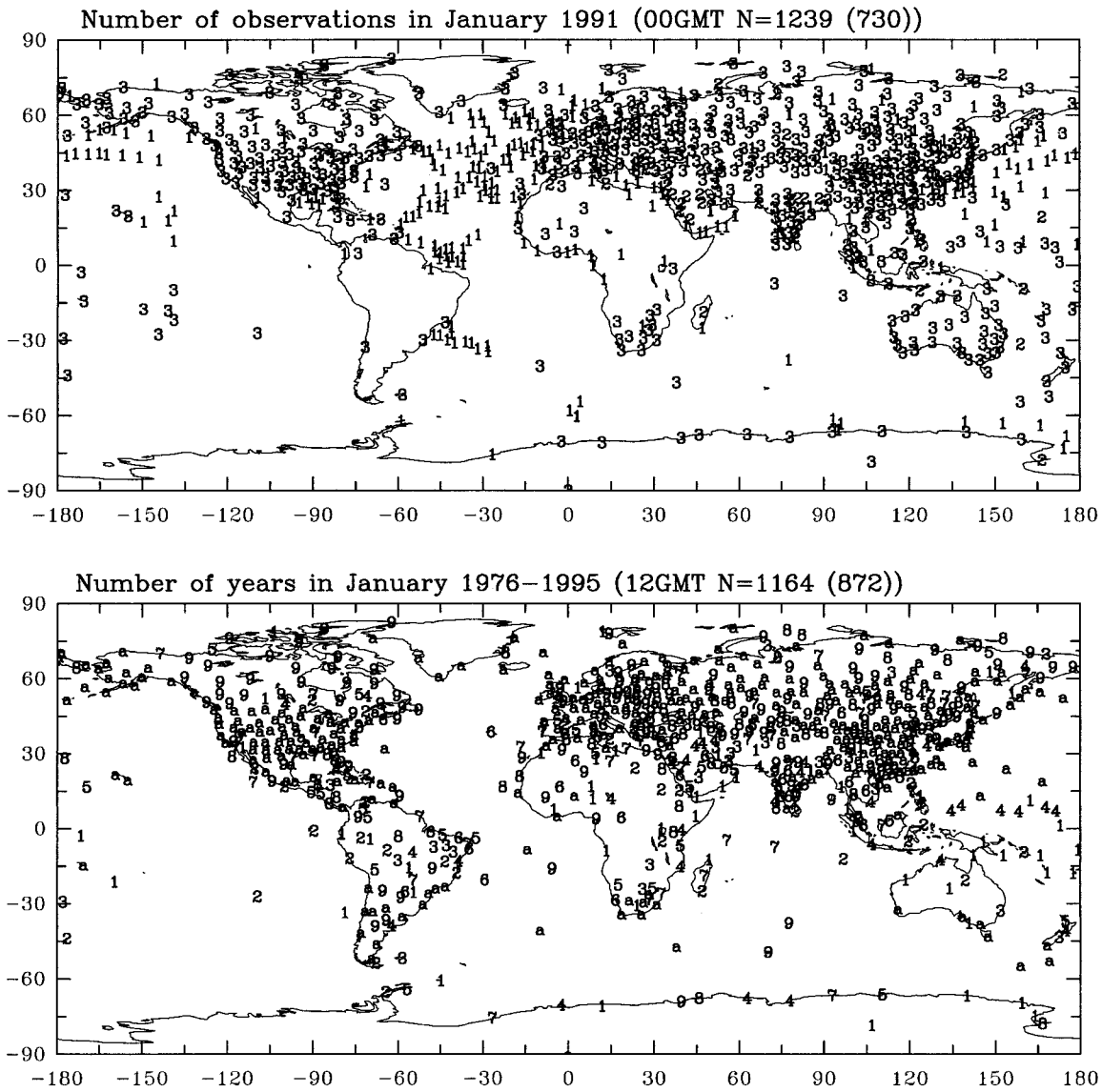

FIG. 1. Geographic distribution of rawinsonde stations at (top) 0000 UTC in Jan 1991 and (bottom) 1200 UTC in Jan from 1976 to 1995. (top) The plotted values indicate number of observations in Jan 1991; ''1'' means less than 10 observations, ''2'' means 10–20 observations, and ''3'' means equal to or more than 20 observations. (bottom) The plotted values indicate number of years of at least 10 humidity observations for Jan covering the 20-yr period: ''1'' indicates 1 and 2 yr, ''2'' for 3 and 4 yr, and so on, and ''a'' indicates 19 and 20 yr. To make numbers readable, only one station in each $2° \times 2°$ (lat by long) box is shown here. Overlapping stations have similar numbers most of time.

tively). The RH threshold was derived based on comparisons of rawinsonde humidity profiles with aircraft observations of cloud-stop and cloud-base heights (Poore et al. 1995) and surface estimates of cloud-base heights (WR95). The RH profile is examined sequentially from the surface to the top to find cloud bases and tops. For ''single-level'' clouds, which have the same level identified as top and base, cloud top is assigned at half the distance to the next level above and cloud base is at half the distance to the next level below.

c. Surface observations

A cloud climatic dataset has been produced from surface weather observations (Hahn et al. 1982, 1984; Warren et al. 1986, 1988), which we refer to as swobs. Swobs provide information on the frequency of occurrence of six cloud types, the probability of co-occurrence of any two of six cloud types, and the frequency of occurrence of a given cloud type without other cloud types. Seasonal mean values of co-occurrence frequency are averages of 10 years of data for 1971–80 over 5°

$\times$ 5° (latitude by longitude) grid boxes over land and for 1965–76 over 15° $\times$ 30° grid boxes over ocean. We estimate the relative frequency of multilayered clouds under cloudy conditions by using the following equation:

$$F_{\text{ml}} = 100 - \frac{\sum_{i=1}^{6} F_i F_{\text{NO}i}}{100 - F_{\text{clear}} - F_{\text{fog}}},$$

where F_{ml} is the frequency of occurrence of multilayered clouds, F_i is the frequency of occurrence of a cloud type, $F_{\text{NO}i}$ is the percent probability of occurrence of a cloud type given that no other clouds are present, and F_{clear} and F_{fog} are frequencies of occurrence of completely clear sky and sky obscured due to fog, respectively. Swobs data over land and ocean are replicated onto a 2.5° $\times$ 2.5° grid. In grid boxes where both ocean and land data are available, only land data are used. The seasonal mean frequency of multilayered clouds from swobs is compared with the CVS dataset in section 3b.

d. Satellite observations

The International Satellite Cloud Climatology Project (ISCCP) D2 cloud data product reports monthly mean cloud amount, top pressure, optical thickness, and liquid water path with a spatial resolution equivalent to 2.5° $\times$ 2.5° at the equator (Rossow et al. 1996). ISCCP cloud-top pressures are compared with those from the CVS dataset in section 3b, and ISCCP liquid water path data are used to study effects of cloud physical thickness on optical thickness in section 5b. The ISCCP dataset also reports a monthly aggregate vertical distribution of cloud-top pressures and the amounts of cloud classified as low, middle, and high by cloud-top pressures. Mean high, middle, and low cloud amounts from ISCCP data are presented in Table 2 in contrast to that from raobs and swobs.

3. Limitations of analysis and results

The results of detailed validation results have been reported in WR95, Wang (1997) and Wang et al. (1999). The uncertainties of the CVS results are only briefly summarized here, based on comparisons of raobs-determined information with that from other available observing systems—conventional surface cloud observations, satellite observations, and surface-based active sensors. These studies include both comparisons of coincident and collocated observations as well as comparisons of statistical results.

a. Uncertainties in cloud detection

The raobs have two major problems detecting cloud layers. In humid marine boundary layers at lower latitudes, the analysis miscategorizes clear moist layers as cloudy layers, tending to underestimate cloud-base heights for the lowest cloud layers. Comparison of cloud detections by raobs and swobs suggests that the raobs analysis overdetects low-level clouds by about 10% (WR95; Wang 1997). Because the air above boundary layer clouds is usually much drier, this problem does not affect detections of low-level cloud tops. Based on direct comparisons with radar and ceilometer data from Atlantic Stratocumulus Transition Experiment (ASTEX), marine boundary layer cloud-base heights are underestimated by 200–300 m in the raobs results (Wang et al. 1999). This difficulty should be less significant in drier continental boundary layers.

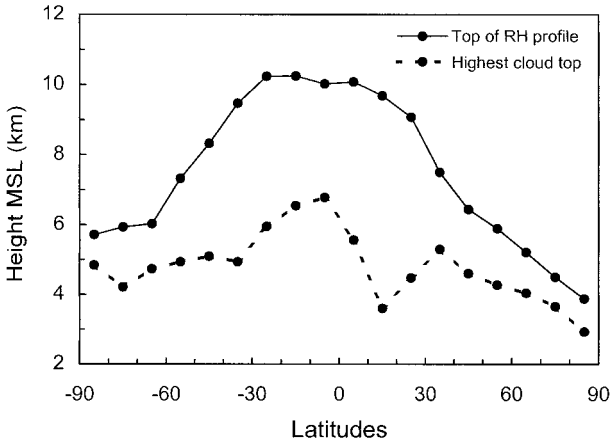

FIG. 2. Latitudinal variations of average top of humidity profiles (km MSL, solid line) and average top of the highest cloud layers (km MSL, dashed line) from the raobs data in Jan 1991.

The second problem is that the rawinsonde humidity sensor loses sensitivity at very cold temperatures. Comparison with a long record of lidar observations collected at Salt Lake City by Sassen and Cho (1992) suggests that the raobs tend to miss about 20%–30% of the highest-level clouds, especially in wintertime; this is equivalent to missing about 5% of all clouds. The missed clouds appear to be both scattered and physically very thin layers (Wang 1997). This effect is exacerbated by coarse vertical resolution in the raobs at higher levels and no humidity reports at temperatures colder than −40°C in the U.S.-type rawinsonde analyses before 1994 (Wade 1994). Thus, the raobs results overestimate cloud-top pressures, especially in regions where cloud tops are frequently colder than −40°C, such as in deep convection and midlatitude cirrus cloud regions (Fig. 4). Coincident and collocated comparison with the ISCCP shows that raobs overestimate the average top pressures of high clouds by about 170 mb, especially in the Tropics (WR95). The −40°C cutoff in humidity reports also limits the top of humidity profiles and then causes biases in latitudinal variations of CVS (Fig. 2). It induces significant biases poleward of 60° latitude in the winter hemisphere, where the top height of the uppermost cloud layer parallels the tops of RH profiles,

while the ISCCP data show slightly increasing cloud-top heights from 70° to 90°N (Rossow and Schiffer 1999).

In addition, the raobs-determined cloud boundaries for tall cumulus and cumulonimbus are likely to be inaccurate, if for no other reasons than the small size of tall cumulus and the generally violent motions in cumulonimbus make rawinsonde measurements unreliable. This problem does not affect the overall statistics, however, because these cloud types are rare, occurring $<10\%$ of the time (Warren et al. 1985; Rossow and Schiffer 1991).

b. Spatial and temporal representativeness of the global CVS dataset

Rawinsonde stations cover 56% of the land area, but only 24% of the oceans (thus only 35% of the globe) (see Fig. 1). This incomplete spatial coverage can bias the average CVS parameters. To estimate the magnitude of the spatial sampling bias, we compare the distribution of monthly mean ISCCP top pressures in 1991, derived from data collocated in the rawinsonde stations, with that from the globally complete ISCCP data (Fig. 3). Over oceans the grid boxes without rawinsonde stations sample fewer cloud tops above $\sim$550 mb but more in the range from 650 to 750 mb in both January and July. Over land, the signs of sampling biases are opposite in January and July. The frequency distribution of monthly mean cloud-top pressures at all rawinsonde stations is also shown in Fig. 3, illustrating the undersampling of clouds with tops above 500 mb by raobs. There is also a significant undersampling of marine boundary layer clouds in July because there are more boundary layer clouds in summer than in winter over open ocean where there are few of rawinsonde stations (cf. Klein and Hartmann 1993).

Sampling error can arise in determining the time-averaged value of a time-varying quantity when the quantity is measured at intervals that are long compared with the characteristic scales of the variations and/or when the available sample population is small. The raobs sampling frequency is, on average, more than once daily, so that with 20 years of data, the sampling and population are more than sufficient to reduce the sampling error associated with synoptic variations to a small fraction of the mean values. An upper limit on the remaining sampling error is obtained by assuming that the measured variations of monthly mean values are caused solely by sampling. Table 1 shows that the values of the standard errors (standard deviation divided by the square root of the number of each month available, 20) are small relative to the mean values. Since there is some real interannual variability, the values shown in Table 1 are overestimates of the actual sampling error.

Although the error in the average results caused by sampling of quasi-random synoptic variations is small, bias and/or errors can occur if there are systematic time variations of the clouds that are not properly sampled. The two main systematic variations of clouds are the seasonal and diurnal cycles (Rossow and Cairns 1995). The former is properly sampled by our dataset, but the latter is not. The twice-daily raobs measurements are an aliased sample of the diurnal cycle, but the magnitude and sign of the error depend on the diurnal phase at which these samples are taken. Unfortunately, collection of raobs at the same synoptic times means that the diurnal phase of the measurements is a systematic function of longitude, for example, 0000 and 1200 UTC correspond about to local midnight and noon in Europe but to local 1800 and 0600 UTC in the central United States. Diurnal cloud cover variations observed from surface (Warren et al. 1986, 1988) and by satellites (Cairns 1995) show the largest amplitude for low-level clouds; however, this amplitude is only 10%–15%. Nevertheless, it should be kept in mind that small geographic differences in our results may be caused, in part, by a varying diurnal bias error.

Despite the sampling biases discussed above, the raobs capture the geographic and seasonal variabilities of CVS according to comparisons of cloud-top pressure and frequency of multilayered cloud with ISCCP and swobs data, respectively (Figs. 4 and 5). Except in deep convective and cirrus cloud regions, raobs and ISCCP have very good agreement on cloud-top pressure; in 62% (64%) of total 3184 (3030) boxes in January (July), the differences are within 100 mb (Fig. 4). The global average difference is 37 mb (23 mb) with a standard deviation of 126 mb (128 mb) in January (July). Raobs show the same general geographic features of cloud-top pressures: higher cloud tops in ITCZ, monsoon, and midlatitude winter storm regions, and low tops in the subsidence region (see Fig. 8). Seasonal variations of cloud-top pressure in term of difference between July and January from raobs also have good agreement with those from ISCCP.

Using swobs data described in section 2c, we estimate the seasonal mean frequency of a multilayered cloud and compare it with that from raobs data (Fig. 5). Several analogous geographic patterns are exhibited by the two datasets: higher frequency in ITCZ regions, lower frequency over Europe–Asia than in North America, and lower values over marine stratocumulus areas. However, raobs report more multilayered clouds in eastern North America, Brazil, and a part of eastern Europe, but less in the tropical western Pacific and southeastern Asia. Here 49% and 53% of a total of 3545 and 3513 boxes have the differences within 10% in DJF (December–January–February, boreal winter) and JJA (June–July–August, boreal summer), respectively, and the average discrepancy from two datasets is -2.57% (-6.33%) (raobs–swobs) with a standard deviation of 15% (16%) in DJF (JJA). The higher frequency of multilayered clouds in swobs than raobs might be partly associated with the fundamental assumption used in the swobs calculation that the probability of an upper cloud (middle

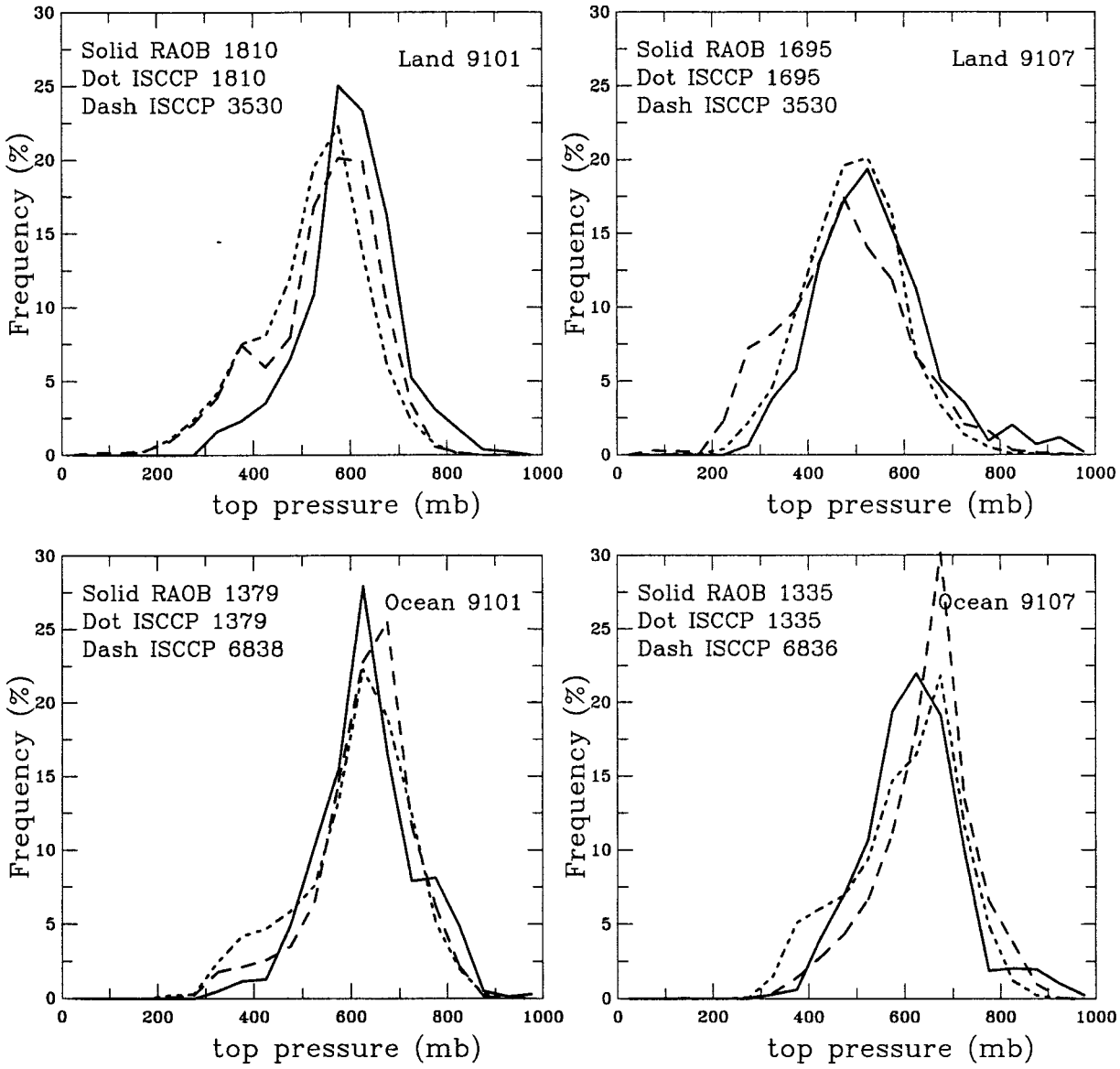

FIG. 3. Frequency distribution of monthly mean cloud-top pressures from raobs-derived CVS data at all rawinsonde stations (solid line), ISCCP data over grid boxes where there are rawinsonde stations (dotted line), and ISCCP data over all grid boxes (dashed line) in Jan and Jul 1991 over land and ocean. Numbers in left corner are number of grid boxes.

or high clouds) is independent of whether a low cloud is overcast (upper cloud cannot be seen) or not (upper cloud can be seen). Good agreement is also found for the magnitudes of seasonal variations of frequency of multilayered clouds (Fig. 5, see discussions in section 4b).

4. Results

The incomplete spatial coverage of global rawinsonde stations (Fig. 1) can bias the calculated global mean values of the CVS parameters, but they still serve as a compact summary of the results. Thus, in the following we emphasize the land–ocean contrasts; as a summary, global mean values are calculated by weighting the separate land and ocean averages in proportion to their areas, approximately 30% and 70%, respectively.

a. Global statistics

Annual mean CVS properties are calculated from the 20-yr CVS dataset and summarized in Table 1. The global, annual mean cloud-top height of the uppermost layers is 5.1 km MSL (584 mb), which is nearly identical to the average from the new version of the ISCCP data, 583 mb (Rossow and Schiffer 1999). This agreement may be coincidental, in part, because of the effects of missed clouds and incomplete spatial coverage on the

TABLE 1. Statistics of annual mean cloud vertical structure parameters over the globe, land, and ocean from the 20-yr data. In each cell, the values in the first, second, and third lines are ones over the globe (G), land (L), and ocean (O). The height is in kilometers above MSL. The last three rows give frequency of one, two, three, and four or more than four-layered clouds. The values in parentheses for global mean are temporal sampling errors based on standard deviations of individual observations in 1985. The similar results are obtained by using data for other years.

Quantity		Height (km)			Pressure (mb)		
		Top	Base	Thickness	Top	Base	Thickness
All clouds	G	4.0 (0.7)	2.4 (0.5)	1.6 (0.4)	665	788	123
	L	4.7	2.8	1.9	612	755	143
	O	3.7	2.3	1.4	687	802	115
Single-layered clouds	G	3.9 (0.6)	1.6 (0.5)	2.3 (0.5)	675	860	186
	L	5.1	2.3	2.7	587	195	208
	O	3.4	1.3	2.1	711	888	177
Two-layered clouds lower layer	G	1.6 (0.3)	0.8 (0.2)	0.8 (0.2)	850	935	85
	L	2.0	1.1	0.9	811	899	88
	O	1.4	0.6	0.8	866	951	85
Higher layer	G	6.2 (0.5)	4.4 (0.4)	1.8 (0.4)	490	610	120
	L	6.9	4.8	2.1	443	576	133
	O	5.9	4.2	1.7	511	625	114
Three-layered clouds lowest layer	G	1.1 (0.2)	0.5 (0.1)	0.6 (0.1)	897	960	63
	L	1.4	0.8	0.6	870	928	58
	O	1.0	0.4	0.6	909	973	65
Middle layer	G	3.4 (0.4)	2.7 (0.3)	0.7 (0.1)	687	748	61
	L	3.6	2.9	0.7	663	726	63
	O	3.3	2.6	0.7	697	758	61
Highest layer	G	6.4 (0.5)	5.3 (0.4)	1.1 (0.2)	476	543	69
	L	6.7	5.5	1.2	451	525	75
	O	6.2	5.2	1.0	486	551	66
Lowest top/lowest base/separation distance	G	5.1 (0.7)	1.2 (0.3)	2.2 (0.4)	584	895	186
	L	5.8	1.9	2.3	530	837	190
	O	4.7	0.9	2.2	607	920	184

		1-layered	2-layered	3-layered	≥4-layered
Frequency (%) of 1/2/3/≥4-layered clouds	G	58	28	9	5
	L	63	27	7	3
	O	56	29	10	5

raobs results, discussed in section 3. The global, annual mean cloud layer thickness, base height of the lowermost cloud layer, and the separation distance between two consecutive layers in multilayered cloud systems, none of which can be derived from any other observations, are 1.6 km (123 mb), 1.2 km MSL (895 mb), and 2.2 km (186 mb), respectively. Cloud-top and cloud-base heights are 1 and 0.5 km larger, respectively, over land than over ocean; as a result clouds are 0.5 km thicker over land than over ocean. The larger cloud heights over land can be accounted for by the height of the land surface, which is about 0.5 km MSL on average, and by more frequent occurrence of low-level cloudiness over ocean. Warren et al. (1986) also notes that the atmospheric boundary layer tends to be at least 0.5 km deeper over land than over ocean.

Globally, 58% of clouds are single-layered and 42% are multilayered; almost 67% of the latter are two-layered clouds. There are about 7% more single-layered clouds over land than ocean; the relative proportion of multilayered clouds that are two-layered is the same over land and ocean. On average, cloud layer thicknesses in multilayered cloud systems are 20%–80% of the average thickness of single-layered clouds, with the lowermost one or two layers having thicknesses $<50\%$ of single-layered clouds. The clear layer thicknesses between two consecutive layers in multilayered cloud systems (e.g., the separation distance) are slightly larger than 2 km, a little thicker than the associated cloud layers.

The frequency distributions of CVS are very similar in shape over land and ocean, except that there are significantly more low-level clouds over ocean (Fig. 6). About one-third of clouds have base heights below 0.5 km, with a nearly uniform distribution above 2 km. The frequency of cloud-top heights decreases rapidly up to about 4 km and then is nearly constant above. Clouds are thinner than 1 km more than half of the time; the broad secondary peak above 5.5 km indicates the occurrence of some very thick clouds. The distribution of the top heights of the uppermost cloud layer is relatively uniform throughout the troposphere with two small maxima near 1.5 and 7.5 km.

For all cloud layers (Fig. 7), the frequency of occurrence tends to decrease with height as found by Wylie and Wang (1997). For two-layered cloud systems, the lowermost layer occurs mostly below 3 km, and the uppermost layer occurs over a wide height range cen-

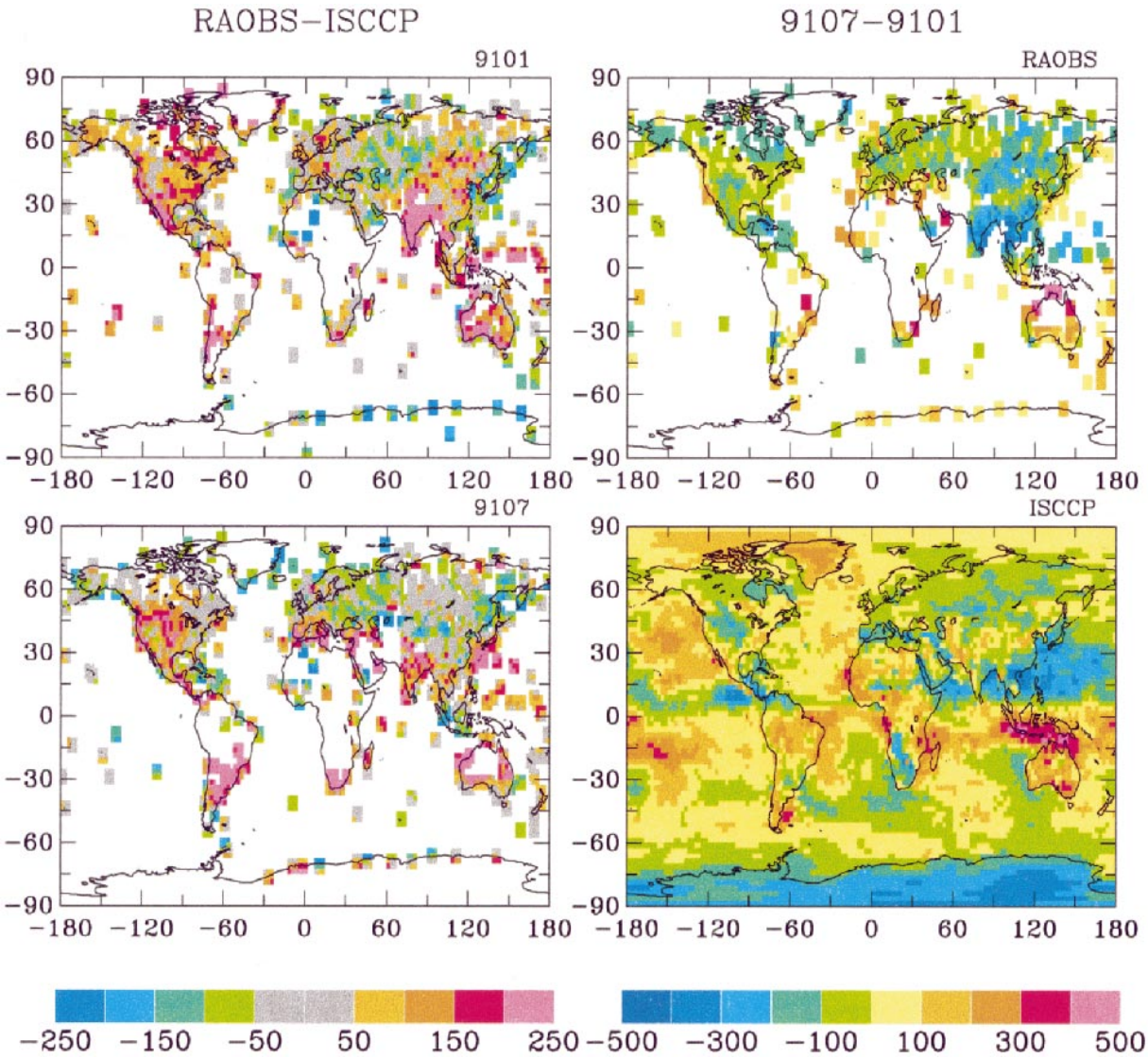

FIG. 4. Geographical distributions of differences in cloud-top pressures from raobs and ISCCP in Jan and Jul 1991 (left panel) and differences between Jul and Jan 1991 for raobs and ISCCP (right panel).

tered on 6–7 km. The lowermost layer of three-layered cloud systems is also located below 3 km, the midlayer height ranges between 1.5 and 7 km, and the uppermost layer ranges from 3 to 10 km with a maximum near 7.5 km. The upper-level cloud layers in multilayered cloud systems tend to be slightly higher over land than over ocean, again probably due to the height of the land topography.

b. Latitudinal and seasonal variations

The tops of uppermost cloud layers are above 500 mb in the ITCZ but below 700 mb in the subsiding regions that are dominated by marine stratocumulus in summer (Fig. 8, Klein and Hartmann 1993; Wang et al. 1998). In Southeast Asia, cloud tops rise from the lower troposphere in wintertime to the upper troposphere in summertime, associated with more frequent deep convective cloud during the summer monsoon (Fig. 8). Cloud tops at midlatitudes in the Northern Hemisphere (NH) move from the midtroposphere in winter associated with storms to the upper troposphere in summer, dominated by more cirrus and some deep convection (cf. Rossow 1993, Fig. 8). The very large average cloud-top heights over the Tibetan Plateau result from the high surface elevation (Fig. 8).

Zonal averaged cloud layer thicknesses increase with latitude and show insignificant differences between DJF and JJA and between land and ocean (not shown). Cloud layers are thickest over northern midlatitude continents, particularly in winter, associated with more vigorous cyclonic storms (Fig. 8). In Southeast Asia, cloud layers

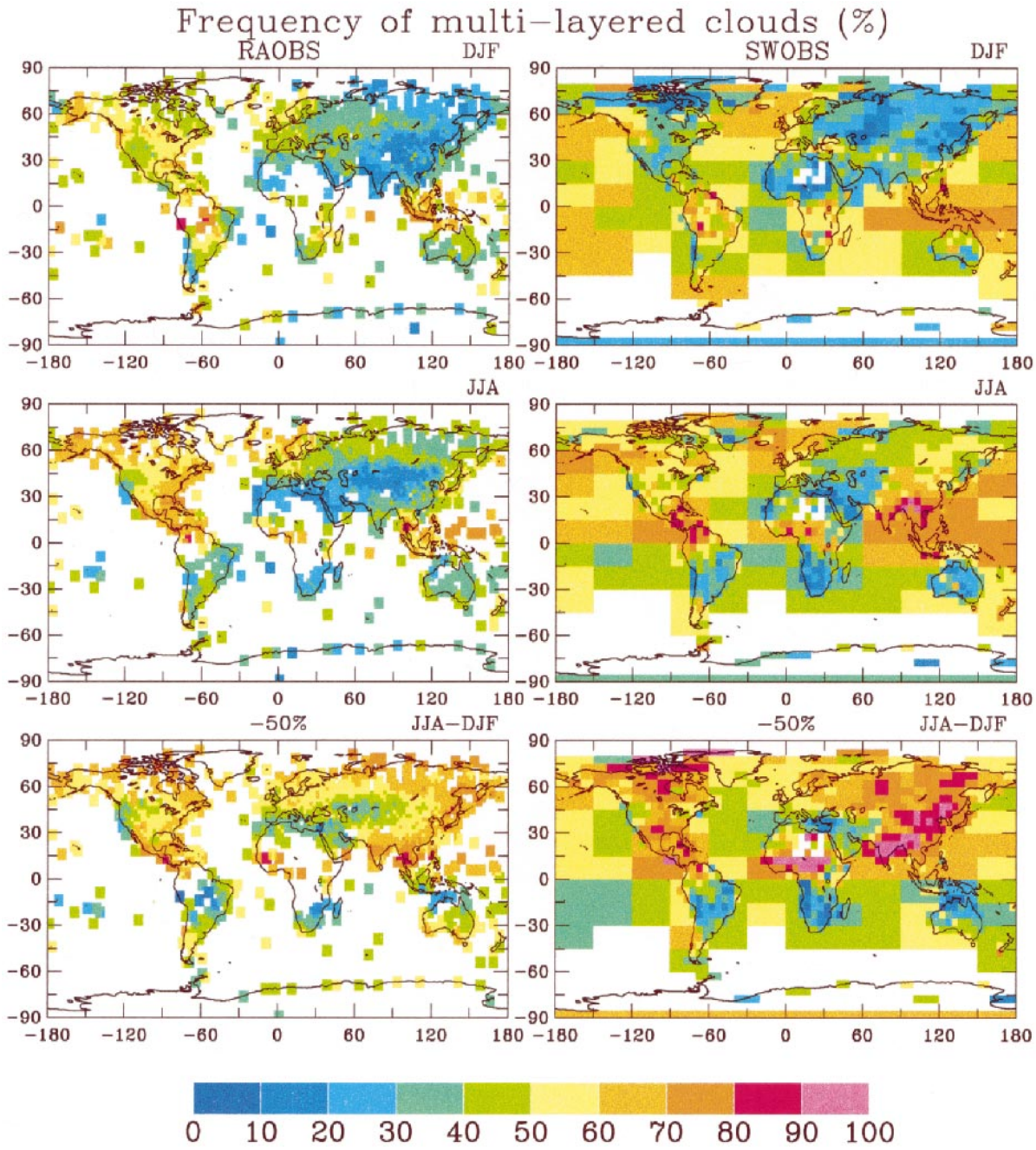

FIG. 5. Global distribution of frequency of occurrence of multilayered clouds (%) in DJF (upper panel) and JJA (middle panel), and the difference between JJA and DJF (lower panel) from raobs (left panel) and swobs (lower panel). The raobs results are derived from 20-yr (1976–95) data. Note that color bar values for the difference should be values shown minus 50%, that is, from −50% to 50%.

are much thicker in summer than winter, corresponding to the appearance of significant deep convective activity in the summer monsoon (Fig. 8).

Multilayered clouds occur most frequently in the Tropics and least frequently in the subtropics; there are more multilayered clouds in summer than in winter and more over ocean than over land in the NH midlatitude (Fig. 9). The geographic distribution of frequency of multilayered cloudiness shows lower frequency in Europe–Asia than in North America, less than 40% of multilayered clouds over the marine stratocumulus regimes, more frequent occurrence off the east coasts of NH continents in JJA and over Southern Hemisphere land areas in DJF and less frequent occurrence over the Mediterranean in summer (Fig. 5).

The lowermost cloud layer in multilayered cloud sys-

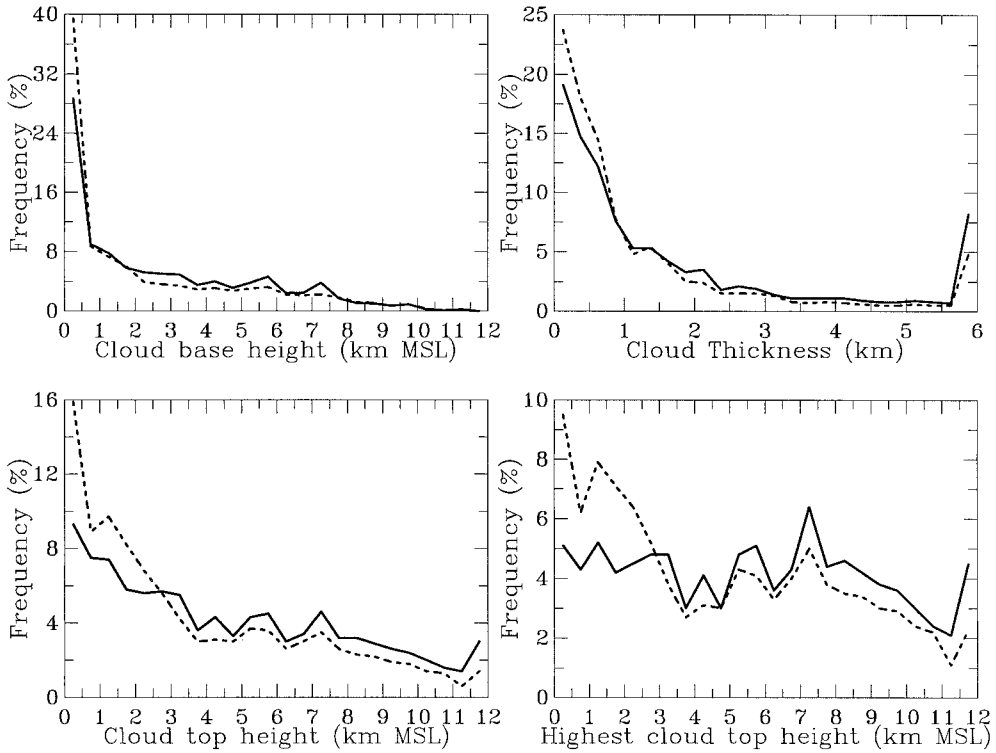

FIG. 6. Frequency distribution of cloud-base and cloud-top heights MSL (km), and layer thicknesses (km) for all cloud layers, and cloud-top height MSL (km) of the highest cloud layers over land (solid line) and ocean (dashed line).

tems almost always occurs below 3 km at all latitudes (not shown), but the upper layer exhibits more interesting variations (Fig. 10). The uppermost layer heights range from 4 to 10 km in the ITCZ, have a bimodal distribution in the subsidence zones with peak frequencies at 2 and 8 km, and are mostly in the upper troposphere at mid- and high latitudes (Fig. 10). The subsidence region distribution suggests the frequent occurrence of double cloud layers in the boundary layer with occasional cirrus above, especially over ocean. Miller et al. (1998) suggested that the double marine boundary layer cloud cases represent decoupled marine boundary layer. The mean relative frequency of single and double cloud layers below 3 km are 74% and 23% in the subsidence regions over ocean, respectively; there are 7% fewer double low clouds over land, suggesting that a decoupled boundary layer occurs much less frequently over land.

The availability of both cloud-base and cloud-top heights in our dataset makes it possible to study the relationship between cloud vertical location and vertical extent, such as two-dimensional frequency distribution of top pressure and layer thickness over NH midlatitude (30°–60°N) land area shown in Fig. 11. The winter season is characterized by three clusters of clouds: thin clouds (layer thicknesses $<$100 mb) occurring below the 800-mb level and above the 500-mb level, corresponding to boundary layer clouds and cirrus; and thicker clouds (layer thicknesses $>$400 mb) with tops above the 600-mb level (Fig. 11). The layer thickness of the thicker clouds linearly increases with decreasing top pressure (Fig. 11). In summer there are more cirrus (thin, high) but less thick clouds. Figure 11 describes a shift from the large, synoptic-scale storm clouds in winter to more frequent fair-weather conditions, particularly over land where more cirrus clouds occur. The cloud structure shown in Fig. 11 qualitatively agrees with the frequency occurrence of cloud optical thickness and cloud-top pressure from ISCCP (Rossow and Schiffer 1991, 1999).

5. Significance of CVS variations and future work

a. Relation of CVS to atmospheric dynamics

The *e*-folding height of clouds estimated from Fig. 7 is around 5 km over ocean and more over land, which is larger than the ''scale height'' for water vapor (about 2.5 km calculated from the global and annual mean in Peixoto and Oort 1992). That the CVS does not follow the vertical structure of water vapor emphasizes the control of the dynamics and clouds with the consequence that clouds do not form most frequently where absolute humidity is highest.

The multilayered clouds always have the lowest layer in the boundary layer, presumably under the control of

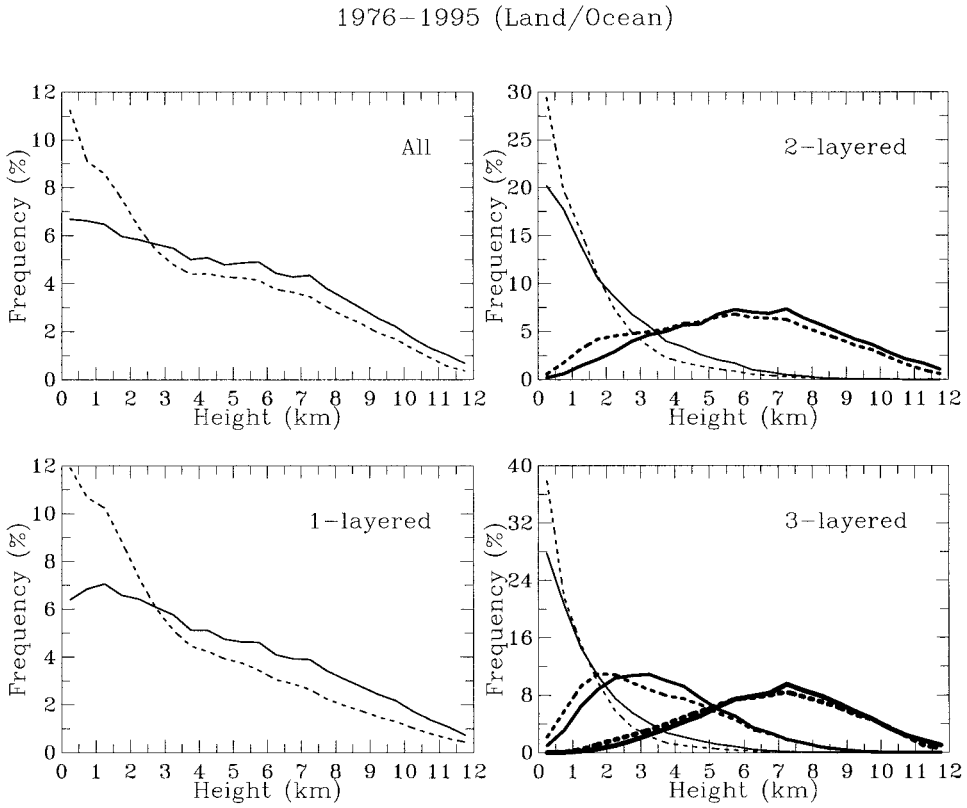

FIG. 7. Frequency distribution of cloud occurrence as a function of height MSL for all cloud layers, single-layered clouds, two-layered cloud systems, and three-layered cloud systems over land (solid lines) and ocean (dashed lines). In two- and three-layered cloud systems, the thin line is for the lowest layer, the thick line is for the middle one, and higher layer in the three- and two-layered systems, respectively, and the thickest line is for the highest layer.

the boundary layer dynamics, but influenced by the large-scale circulation. Given this background of low-level clouds, the large-scale circulation is better revealed by the upper-level clouds. There are very interesting correspondences of the height dependence with the Hadley regime and the storm tracks (see Fig. 10). The maximum of cloud occurrence in the upper troposphere is near the equator and its shift from 0°–10°N in boreal summer to 0°–30°S in austral summer marking the ITCZ and the upwelling part of the Hadley circulation. The subsidence portion of the Hadley circulation is likewise marked by corresponding maxima in the boundary layer between 10°–20°S in boreal summer and between 10°–20°N in austral summer (Fig. 10). The storm tracks are revealed by more frequent thicker and multilayered clouds in the wintertime northern midlatitudes as contrasted with a higher frequency of high, thin layers in summertime.

b. Role of cloud physical thickness variations in cloud optical thickness feedback

Satellite observations of cloud optical thickness variations have suggested a systematic dependence on temperature in low-level clouds (Tselioudis et al. 1992) that implies an important cloud-radiative feedback (Tselioudis et al. 1993). The combination of CVS and meteorological information in our dataset makes possible the study of variations of cloud physical thickness with temperature to help understand its role in controlling variations of cloud optical thickness. The mean latitudinal variation of total cloud physical thickness (the sum of thicknesses of each cloud layer for multilayered clouds) has similar shape to that of cloud water path from the ISCCP D2 data (Fig. 12), suggesting that this particular variation of cloud water path (and optical thickness) with temperature can be attributed, in part, to variations of cloud layer physical thickness. Nevertheless, there are also differences in the relative magnitude of the variations, especially in the polar regions, which indicate that there are also important variations of cloud water content.

A mean cloud liquid water content (LWC) can be estimated from Fig. 12 by dividing the mean liquid water path (LWP = 92 g m^{-2}) by the mean total cloud layer thickness (ΔZ = 1.92 km), giving 0.05 g m^{-3}. This value is smaller than typical LWC values summarized by Cotton and Anthes (1989), which range from

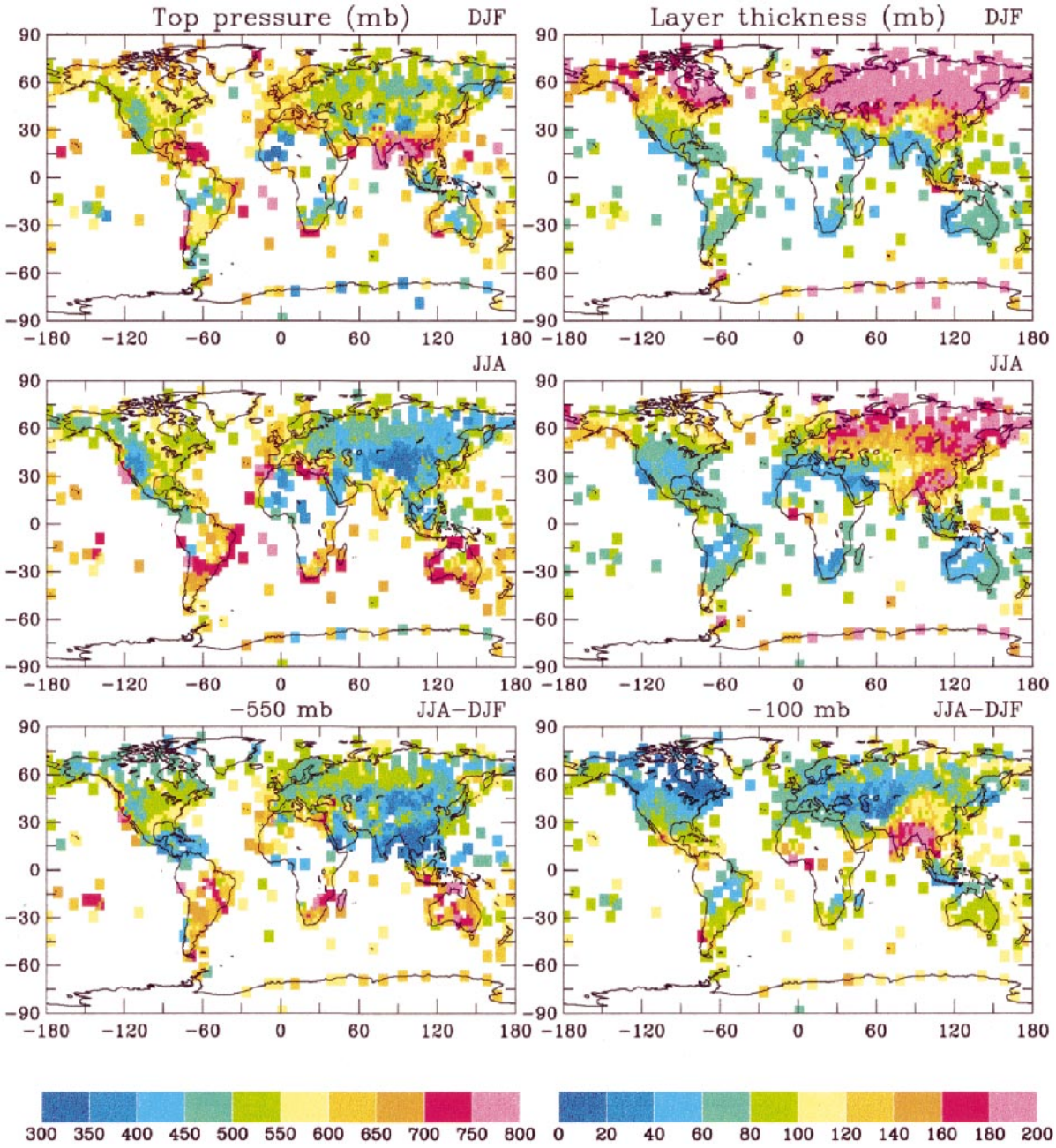

FIG. 8. Global distribution of cloud-top pressures (mb) of the highest cloud layer (left panel) and mean layer thickness (mb) for all cloud layers (right panel) in DJF (upper panel) and JJA (middle panel), and differences between JJA and DJF (lower panel). Color bar values for the differences should be the values shown minus 550 mb (from −250 to 250 mb) for cloud-top pressures, and minus 100 mb (from −100 to 100 mb) for cloud-layer thickness.

0.05 to 0.25 g m^{-3} for stratus and stratocumulus clouds up to 1.5–4.5 g m^{-3} for cumulonimbus clouds. However, the total cloud thickness includes the effects of the frequent multilayer clouds and also includes ice-phase clouds, so a better estimate would be to use the average layer thickness for *warm* clouds (with top temperatures more than 0°C). The average single-layer thickness for warm clouds is about 800 m, which implies an average LWC of about 1.2 g m^{-3}, right in the middle of the range given by Cotton and Anthes for nonprecipitating cloud types. Note that precipitating cloud types are relatively rare (cf. Lin and Rossow 1997) and the raobs likely undersample cumulonimbus. If the mode values of LWP and layer thickness are used, rather than their average values, the implied LWC is only slightly larger. Further detailed comparisons of our layer thickness re-

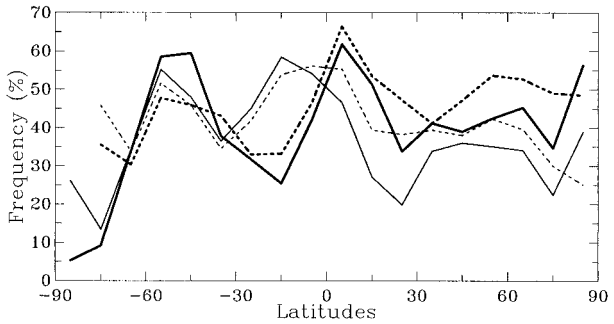

FIG. 9. Latitudinal variations of frequency of multilayered clouds over land (solid lines) and ocean (dashed lines) in DJF (thin line) and JJA (thick line).

sults with individually matched ISCCP and microwave measurements (where possible) of cloud water path are warranted to quantify better the relationships of systematic variations of cloud physical and optical thickness with temperature and other meteorological conditions.

c. Resolving CVS in GCMs

One of the uses of information on CVS is to improve and to validate GCM-predicted clouds. The frequency of multilayered clouds from observations (Fig. 5) has a similar geographic distribution as that from the Goddard Institute for Space Studies GCM (Wang 1997), but the model values are only about half of those from raobs and swobs. This bias cannot be simply attributed to coarse vertical resolution because the model's resolution of about 100 mb seems sufficient to represent the average cloud layer thicknesses and separation distances in multilayered clouds (even though the mode of the distributions of cloud layer thicknesses and separations distances is somewhat smaller). However, the atmospheric circulation in a GCM is also sensitive to vertical profile of radiative heating induced by a cloud, causing a dipole structure with radiative heating near cloud base and cooling at cloud top (both longwave effects, sunlight adds a smaller heating more uniformly distributed over the cloud layer) (Wang and Rossow 1998). This

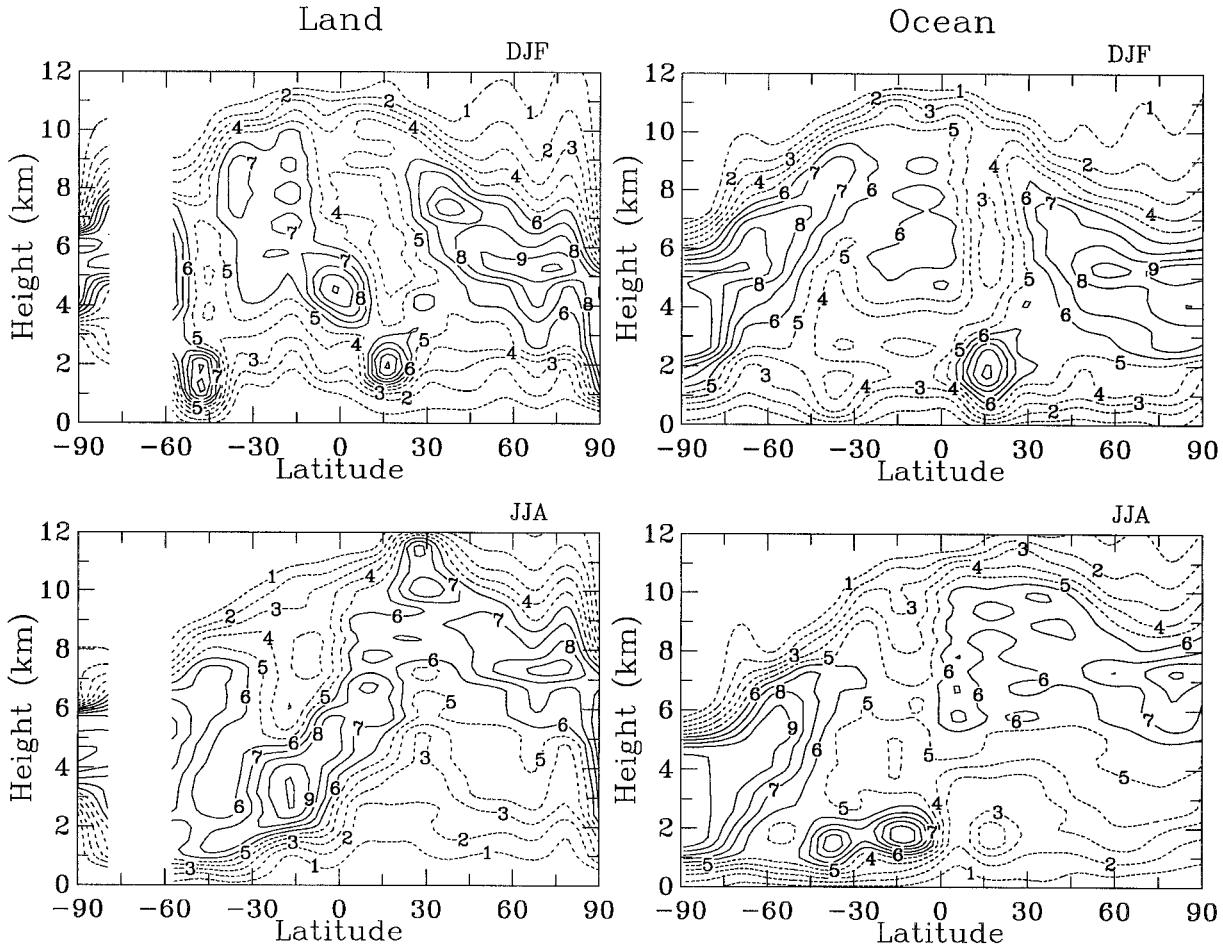

FIG. 10. The frequency distribution of occurrence of cloudiness as a function of latitudes for the higher layer of two-layered cloud systems over land (left panels) and ocean (right panels) in DJF and JJA. The dotted contours are for frequency less than 5%.

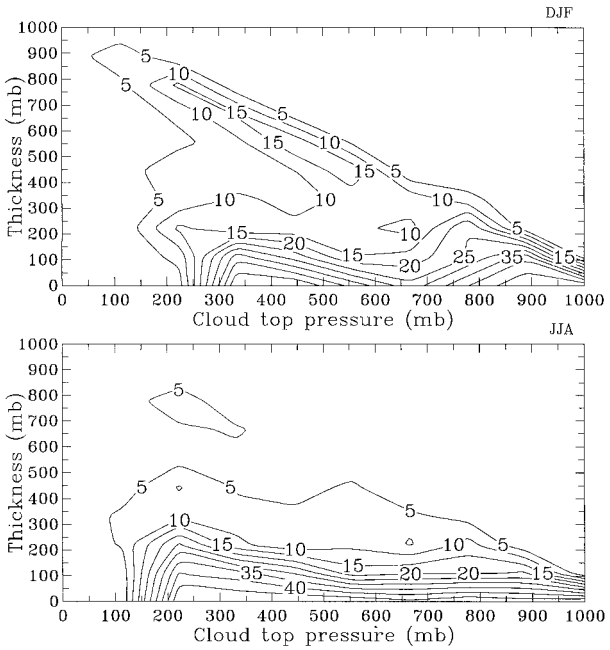

FIG. 11. Two-dimensional frequency distribution of cloud-top pressure (mb) and layer thickness (mb) of the highest cloud layers in the NH midlatitude (30°–60°N) land in DJF and JJA. The frequencies in percent are relative to the maximum values.

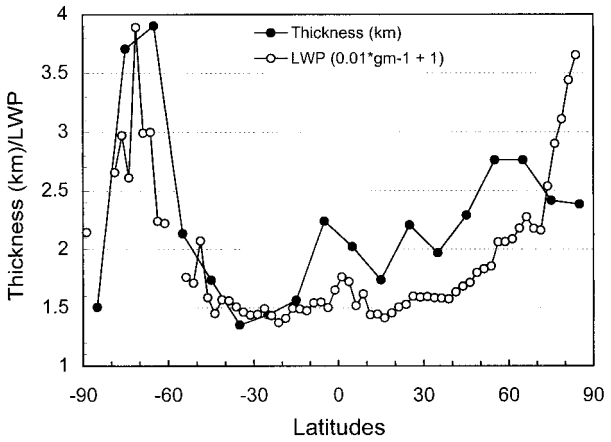

FIG. 12. Latitudinal variations of total cloud thickness (km) over land from 1-yr (1990) raobs data and LWP over land from 1-yr (1990) ISCCP D2 data collocated to rawinsonde stations. The values of LWP shown here are LWP (gm^{-2}) multiplied by 0.01 and then added by 1 unit.

result suggests that, in addition to resolving the cloud layers and their vertical separation, the models may need to represent each cloud layer by two model layers to capture this dipole structure and its effect on layer thickness and cloud structure. That would require a model vertical resolution of at least 50–60 mb (see Table 1) or about 14 layers in the troposphere. Since the average cloud layer thickness in the marine boundary layer is substantially smaller still, more resolution is needed there.

Table 2 compares the layer cloud amounts (normalized by total cloud cover) reported by three cloud climatologies: the surface-based cloud observations (Warren et al. 1986, 1988), the satellite-based ISCCP results (Rossow and Schiffer 1999), and our raobs-based results, representing the currently available information on cloud vertical structure. Results in Table 2 can be used for validating a GCM's cloud scheme. If cloud layer occurrences were truly random, that is, uncorrelated, meaning that there is no systematical vertical structure, then all three datasets should agree on the average layer cloud amounts when corrected for sampling frequency at each level (assuming no other measurement biases). The surface observations have been corrected for their ''bottom-up'' view by using the observed cooccurrence statistics (Warren et al. 1985); we show the ISCCP results adjusted for their ''top-down'' view by assuming random layer overlap. The notable disagreements mean that clouds do have systematic vertical structures in some locations, that is, the occurrences

TABLE 2. Annual mean high, middle, and low cloud amounts normalized by total cloud amounts in four latitude zones over land and ocean from raobs, ISCCP, and swobs. The ISCCP data are from 1990 to 1992. The mid and low-level ISCCP cloud amounts have been adjusted assuming random overlap; high-level cloud amounts do not change.

	Land				Ocean			
	15°S–15°N	15°–35°N	35°–65°N	65°–90°N	15°S–15°N	15°–35°N	35°–65°N	65°–90°N
High cloud								
raobs	48	52	57	52	45	34	46	46
ISCCP	51	47	40	21	53	32	27	12
swobs	69	61	68	62	60	48	48	54
Middle cloud								
raobs	44	29	33	36	34	24	32	35
ISCCP adjusted	38	45	52	51	35	30	42	46
swobs	53	44	49	55	53	48	58	57
Low cloud								
raobs	67	56	54	57	86	82	72	70
ISCCP adjusted	50	54	57	64	48	66	71	73
swobs	60	46	45	46	79	80	79	59

of clouds at different levels are correlated, at least in part, with meteorological conditions. The agreement at some latitudes is misleading because of the averages over time and longitude. Moreover, the cooccurrence statistics from swobs do not necessarily indicate layer overlap because what a surface observer actually reports is the cooccurrence of two different layers of cloud *in different parts of the sky*. Only the raobs dataset actually measures cloud vertical structure in an atmospheric column, providing a more accurate representation of cloud vertical structure (subject to the limitations discussed in section 3). Thus, we see in Table 2 that the amount of low-level clouds reported by raobs and swobs is often larger than in the satellite dataset with its top-down view, especially over ocean, but smaller in the polar land areas. Mid-level cloud amounts from the three datasets present a more confusing pattern. Given that all three of these datasets have some important measurement biases, the single best (statistical) description of cloud vertical structure will come from a combined analysis of these three datasets, after reconciling the effects of measurement errors. This will require a more thorough study of the differences among these datasets.

d. Future work

There are three major limitations in using raobs to determine CVS. 1) The degraded sensitivity of the humidity sensors at temperatures much below −40°C causes many thin and high-level clouds to be missed, especially isolated cirrus, and the top heights of some high-level clouds to be underestimated. 2) The ambiguity of detecting cloud bases in very humid marine boundary layers causes some overdetection that leads to an underestimate of cloud-base heights. 3) The current raobs dataset provides poor coverage of the ocean, particularly in the Southern Hemisphere, and inadequate diurnal sampling.

To remedy the first limitation, improvements in rawinsonde humidity sensors are essential as well as routine archival of the data with higher vertical resolution. The new practice of reporting humidity below −40°C for U.S.-type rawinsondes, starting in October 1993 (Wade 1994) and the availability of high vertical resolution (~100 m or less) data offer prospects for improving the detection of high-level and polar clouds (Hamilton and Vincent 1995). Raising the RH threshold used in our analysis method can partly solve the second problem, as suggested by the comparison study during ASTEX (Wang et al. 1999). More collection of ship rawinsonde observations and the possible future dropwindsonde observations from aircraft over ocean (Douglas and Stensrud 1996) may improve ocean coverage. The limitation on diurnal sampling can only be removed by routinely making more frequent soundings, at least four per day; but this is unlikely given the current expense—in fact, the number of reporting stations in the observing network appears to be declining.

The raobs CVS results provide a very valuable addition to the study of cloud–radiation–dynamics interactions, particularly if combined with surface weather observations and satellite measurements of atmospheric and cloud properties. Further work with such data combinations for specific meteorological conditions and particular types of clouds will help to advance our understanding of cloud processes. In addition, the CVS dataset can be employed with satellite cloud datasets and a radiative transfer model to calculate more realistic radiative flux profiles by replacing single cloud layers (e.g., Rossow and Lacis 1990; Zhang et al. 1995) with more realistic CVS. However, although our raobs CVS can be used to make important progress in all these types of studies, the results will still be limited by the lack of information about the vertical distribution of cloud water *mass* and its microphysical characteristics (phase, particle size, and shape).

Although the raobs dataset provides a rich collection of information about the variations of cloud vertical structure and can be exploited in a ''case study compositing'' approach (like Lau and Crane 1995) to examine cloud vertical structure associated with different meteorological situations, we still need to obtain information that is globally complete and that resolves the dynamical variations within cloud systems in more detail. Now approved for launch in 2003 are two satellite missions that fly a lidar (Picasso–Cena) and a cloud radar (CloudSat). By combining these new observations with the higher time resolution and more extensive spatial coverage provided by the ISCCP dataset, we should be able to assemble a quantitative description of the dynamic variations of the three-dimensional structure of cloud systems.

Acknowledgments. We would like to thank Drs. Roy Jenne and Abraham H. Oort for providing the global rawinsonde data. J. Wang is grateful to Dr. J. Curry at the University of Colorado for support to finish this study. This work is also supported by the NASA Climate and Radiation Program managed by Dr. Robert A. Curran and National Science Foundation under Grant 962937.

REFERENCES

Baum, B. A., B. A. Wielicki, P. Minnis, and S. C. Tasy, 1994: Multilevel cloud retrieval using multispectral HIRS and AVHRR data: Nighttime oceanic analysis. *J. Geophys. Res.,* **99,** 5499–5514.

Cairns, B., 1995: Diurnal variations of cloud from ISCCP data. *Atmos. Res.,* **37,** 133–246.

Cotton, W. R., and R. A. Anthes, 1989: *Storm and Cloud Dynamics.* International Geophysics Series, Vol. 44, Academic Press, 883 pp.

Douglas, M. W., and D. J. Stensrud, 1996: Upgrading the North American upper-air observing network: What are the possibilities? *Bull. Amer. Meteor. Soc.,* **77,** 907–924.

Hahn, C. J., S. G. Warren, J. London, R. M. Chervin, and R. Jenne,

1982: Atlas of simultaneous occurrence of different cloud types over ocean. NCAR Tech. Note TN-201+STR, 212 pp.

——, ——, ——, ——, and ——, 1984: Atlas of simultaneous occurrence of different cloud types over land. NCAR Tech. Note TN-241+STR, 211 pp.

Hamilton, K., and R. A. Vincent, 1995: High-resolution radiosonde data offer new prospects for research. *Eos, Trans. Amer. Geophys. Union,* **76,** 497–507.

Hughes, N. A., 1984: Global cloud climatologies: A historical review. *J. Climate Appl. Meteor.,* **23,** 724–751.

Jin, Y., and W. B. Rossow, 1997: Detection of cirrus overlapping low-level clouds. *J. Geophys. Res.,* **102,** 1727–1737.

Klein, S. A., and D. L. Hartmann, 1993: The seasonal cycle of low stratiform clouds. *J. Climate,* **6,** 1587–1606.

Kropfli, R. A., and Coauthors, 1995: Cloud physics studies with 8 mm wavelength radar. *Atmos. Res.,* **35,** 299–314.

Lau, N.-C., and M. W. Crane, 1995: A satellite view of the synoptic-scale organization of cloud properties in midlatitude and tropical circulation systems. *Mon. Wea. Rev.,* **123,** 1984–2006.

Lin, B., and W. B. Rossow, 1997: Precipitation water path and rainfall rate estimates over oceans using special sensor microwave imager and International Satellite Cloud Climatology Project data. *J. Geophys. Res.,* **102,** 9359–9374.

——, P. Minnis, B. Wielicki, D. R. Doelling, R. Palikonda, D. F. Young, and T. Uttal, 1998: Estimation of water cloud properties from satellite microwave, infrared, and visible measurements in oceanic environments. Part 2: Results. *J. Geophys. Res.,* **103,** 3887–3906.

Miller, M. A., M. P. Jensen, and E. E. Clothiaux, 1998: Diurnal cloud and thermodynamic variations in the stratocumulus transition regime: A case study using in situ and remote sensors. *J. Atmos. Sci.,* **55,** 2294–2310.

Peixoto, J. P., and A. H. Oort, 1992: *Physics of Climate.* American Institute of Physics, 520 pp.

——, and ——, 1996: The climatology of relative humidity in the atmosphere. *J. Climate,* **9,** 3443–3463.

Platt, C. M. R., and Coauthors, 1994: The Experimental Cloud Lidar Pilot Study (ECLIPS) for cloud–radiation research. *Bull. Amer. Meteor. Soc.,* **75,** 1635–1654.

Poore, K., J. Wang, and W. B. Rossow, 1995: Cloud layer thicknesses from a combination of surface and upper-air observations. *J. Climate,* **8,** 550–568.

Randall, D. A., Harshvardhan, D. A. Dazlich, and T. G. Corsetti, 1989: Interactions among radiation, convection, and large-scale dynamics in a general circulation model. *J. Atmos. Sci.,* **46,** 1943–1970.

Rind, D., and W. B. Rossow, 1984: The effects of physical processes on the Hadley circulation. *J. Atmos. Sci.,* **41,** 479–507.

Rossow, W. B., 1993: Satellite observations of radiation and clouds to diagnose energy exchanges in the climate: Parts I and II. *Energy and Water Cycles in the Climate System,* E. Raschke and D. Jacob, Eds., NATO ASI Series, Vol. I5, 123–164.

——, and A. A. Lacis, 1990: Global, seasonal cloud variations from satellite radiance measurements. Part II: Cloud properties and radiative effects. *J. Climate,* **3,** 1204–1253.

——, and R. A. Schiffer, 1991: ISCCP cloud data products. *Bull. Amer. Meteor. Soc.,* **72,** 2–20.

——, and B. Cairns, 1995: Monitoring changes of clouds. *Climatic Change,* **31,** 175–217.

——, and R. A. Schiffer, 1999: Advances in understanding clouds from ISCCP. *Bull. Amer. Meteor. Soc.,* **80,** 2261–2287.

——, A. W. Walker, D. E. Beuschel, and M. D. Roiter, 1996: International Satellite Cloud Climatology Project (ISCCP) documentation of new cloud datasets. WMO/TD-737, World Meteorological Organization, Geneva, Switzerland, 115 pp.

Sassen, K., 1991: The polarization lidar technique for cloud research: A review and current assessment. *Bull. Amer. Meteor. Soc.,* **72,** 1848–1866.

——, and B. S. Cho, 1992: Subvisual-thin cirrus lidar dataset for satellite verification and climatological research. *J. Appl. Meteor.,* **31,** 1275–1285.

Sheu, R.-S., J. Curry, and G. S. Liu, 1997: Vertical stratification of tropical cloud properties as determined from satellite. *J. Geophys. Res.,* **102,** 4231–4246.

Slingo, A., and J. M. Slingo, 1988: The response of a general circulation model to cloud longwave radiative forcing. I: Introduction and initial experiments. *Quart. J. Roy. Meteor. Soc.,* **114,** 1027–1062.

Slingo, J. M., and A. Slingo, 1991: The response of a general circulation model to cloud longwave radiative forcing. II: Further studies. *Quart. J. Roy. Meteor. Soc.,* **117,** 333–364.

Stephens, G. L., 1978: Radiation profiles in extended water clouds. I: Theory. *J. Atmos. Sci.,* **35,** 2111–2122.

Tselioudis, G., W. B. Rossow, and D. Rind, 1992: Global patterns of cloud optical thickness variation with temperature. *J. Climate,* **5,** 1484–1495.

——, A. A. Lacis, D. Rind, and W. B. Rossow, 1993: Potential effects of cloud optical thickness on climate warming. *Nature,* **366,** 670–672.

Uttal, T., E. E. Clothiaux, T. P. Ackerman, J. M. Intrieri, and W. L. Eberhard, 1995: Cloud boundary statistics during FIRE II. *J. Atmos. Sci.,* **52,** 4276–4284.

Wade, C. G., 1994: An evaluation of problems affecting the measurement of low relative humidity on the United States radiosonde. *J. Atmos. Oceanic Technol.,* **11,** 687–700.

Wang, J., 1997: Determination of cloud vertical structure from upper air observations and its effects on atmospheric circulation in a GCM. Ph.D. dissertation, Columbia University, 233 pp. [Available from J. Wang, NCAR/SSSF, P.O. Box 3000, Boulder, CO 80307-3000.]

——, and W. B. Rossow, 1995: Determination of cloud vertical structure from upper-air observations. *J. Appl. Meteor.,* **34,** 2243–2258.

——, and ——, 1998: Effects of cloud vertical structure on atmospheric circulation in the GISS GCM. *J. Climate,* **11,** 3010–3029.

——, ——, T. Uttal, and M. Rozendaal, 1999: Variability of cloud vertical structure during ASTEX observed from a combination of rawinsonde, radar, ceilometer, and satellite. *Mon. Wea. Rev.,* **127,** 2484–2502.

Warren, S. G., C. J. Hahn, and J. London, 1985: Simultaneous occurrence of different cloud types. *J. Climate Appl. Meteor.,* **24,** 658–667.

——, ——, R. M. Chervin, and R. L. Jenne, 1986: Global distribution of total cloud cover and cloud type amounts over land. NCAR Tech. Note NCAR/TN-273+STR, 29 pp. and 200 maps.

——, ——, J. London, R. M. Chervin, and R. L. Jenne, 1988: Global distribution of total cloud cover and cloud type amounts over ocean. NCAR Tech. Note NCAR/TN-317+STR, 42 pp. and 170 maps.

Webster, P. J., and G. L. Stephens, 1984: Cloud–radiation interaction and the climate problem. *The Global Climate,* J. Houghton, Ed., Cambridge University Press, 63–78.

Wylie, D. P., and P.-H. Wang, 1997: Comparison of cloud frequency data from the high-resolution infrared radiometer sounder and the Stratospheric Aerosol and Gas Experiment II. *J. Geophys. Res.,* **102,** 29 893–29 900.

Zhang, Y.-C., W. B. Rossow, and A. A. Lacis, 1995: Calculation of surface and top-of-atmosphere radiative fluxes from physical quantities based on ISCCP datasets. Part I: Method and sensitivity to input data uncertainties. *J. Geophys. Res.,* **100,** 1149–1165.